

## PAPER



Cite this: *Soft Matter*, 2016,  
12, 5818

## Capillary driven flow of polydimethylsiloxane in open rectangular microchannels†

Timothy W. Sowers,<sup>a</sup> Rohit Sarkar,<sup>b</sup> Suhas Eswarappa Prameela,<sup>b</sup> Ehsan Izadi<sup>a</sup> and Jagannathan Rajagopalan<sup>\*ab</sup>

The flow of liquid polydimethylsiloxane (PDMS, Dow Corning Sylgard 184, 10:1 base to cross-linker ratio) in open, rectangular silicon microchannels, with and without a coating (100 nm) of poly-tetrafluoro-ethylene (PTFE), was studied. Photolithographic patterning and etching of silicon wafers was used to create microchannels with a range of widths (~5–50 μm) and depths (5–20 μm). Experimental PDMS flow rates in both PTFE-coated and uncoated channels were compared to an analytical model based on the work of Lucas and Washburn. The experimental flow rates matched the predicted flow rates reasonably well when the channel aspect ratio (width to depth),  $p$ , was less than 2. For channels with  $p > 2$ , the observed flow rates progressively lagged model predictions with increasing  $p$ . The experimental data, including zero flow rates in certain high aspect ratio PTFE-coated channels, can largely be explained by changes in the front and upper meniscus morphology of the flow as the channel aspect ratio is varied. The results strongly suggest that meniscus morphology needs to be taken into account to accurately model capillary flow in microchannels, especially those with large aspect ratios.

Received 14th April 2016,  
Accepted 6th June 2016

DOI: 10.1039/c6sm00897f

www.rsc.org/softmatter

### 1. Introduction

Soft polymeric materials have found widespread applications in biology and medicine. They are used to fabricate microfluidic devices for cell sorting and biochemical assays,<sup>1</sup> as substrates for studying cell mechanobiology,<sup>2</sup> and as implants and substrates for tissue engineering.<sup>3,4</sup> Among polymeric materials, polydimethylsiloxane (PDMS) is perhaps most widely used because of its low Young's modulus,<sup>5</sup> wide operating temperature range,<sup>6</sup> optical transparency and biocompatibility.<sup>7</sup> Arrays of PDMS microstructures have been used to measure cellular forces,<sup>8,9</sup> which directly affect cell growth and migration,<sup>10</sup> and PDMS cantilevers have been used to measure contractile forces of muscle cells.<sup>11,12</sup> More broadly, PDMS based devices are increasingly used to study the effect of the mechanical microenvironment on cell and tissue behavior<sup>13–16</sup> and develop biohybrid systems.<sup>17</sup>

There are several methods to fabricate PDMS microstructures and devices. One particularly powerful method is capillary micromolding, which can be used to fabricate PDMS microstructures in a reliable and repeatable manner.<sup>18,19</sup> In capillary micromolding,

a network of microchannels is first formed by either etching the substrate or by placing an elastomeric mask on top of the substrate. Liquid polymer is then placed at the entrance of the channels and is drawn in by capillary action. The polymer is finally cured and the solidified structures are released from the substrate.

Recently, capillary micromolding has been used to fabricate millimetre long PDMS filaments that have width and depths <10 μm. These filaments have extremely low stiffness (<0.1 pN μm<sup>-1</sup>) and can be employed as high resolution force sensors or as scaffolds for biohybrid devices.<sup>7,17</sup> However, as the filaments become thinner, the substrate must be coated with a non-adhesive layer (*e.g.* Teflon) to ensure that the filaments are not damaged during removal. This non-adhesive layer significantly slows the capillary driven flow of liquid PDMS, which ultimately constrains the possible filament geometries. Thus, it is essential to understand the dynamics of PDMS flow in microchannels to quantify the limits of capillary micromolding for fabricating PDMS microstructures.

Generally, the flow behaviour of Newtonian fluids in open rectangular microchannels follows the Lucas–Washburn<sup>20,21</sup> equation, which predicts that the square of the distance travelled is proportional to time. For a given surface, it is known that the width, depth, and width to depth ratio ( $p$ ) of the channel affect the flow rate. But only a few studies have experimentally examined the effect of these parameters on the capillary driven flow of PDMS. One study has revealed that the channel filling time is sensitive to channel depth only up to a certain threshold for a given width.<sup>22</sup>

<sup>a</sup> Department of Mechanical and Aerospace Engineering, School for Engineering of Matter Transport and Energy, Arizona State University, Tempe, AZ – 85287, USA. E-mail: jrajago1@asu.edu

<sup>b</sup> Department of Materials Science and Engineering, School for Engineering of Matter Transport and Energy, Arizona State University, Tempe, AZ – 85287, USA

† Electronic supplementary information (ESI) available. See DOI: 10.1039/c6sm00897f

Another study has theorized the effect of forward meniscus morphologies on flow rate<sup>23</sup> in vertical microchannels. Other researchers have measured the effect of forward meniscus morphologies in rough *versus* smooth microchannels<sup>24</sup> at very short time scales. Several analytical and numerical models for capillary flow in microchannels have also been proposed.<sup>23,25,26</sup> But a complete understanding of how different parameters affect capillary flow rate is currently lacking. In particular, the effect of meniscus morphology on viscous dissipation and, consequently, on the flow rates in microchannels has not been studied.<sup>23</sup>

In this work, experiments are performed to measure flow rates of liquid PDMS in open, rectangular microchannels with nominal depths of 5–20  $\mu\text{m}$  and widths of 5–50  $\mu\text{m}$ . Particular attention is focused on elucidating the effect of upper and forward meniscus morphology on the flow behaviour and the observed flow rates are compared to a model<sup>25</sup> based on the Lucas–Washburn equation.<sup>20,21</sup> The experimental flow rates reasonably match the predicted flow rates when the aspect ratio  $p$  is small ( $\leq 2$ ). However, the experimental flow rates increasingly lag the predicted flow rates as  $p$  increases. The experimental data is largely explained by changes in the front and upper meniscus morphology of the flow as the channel aspect ratio is varied.

## 2. Methods and model

### Microchannel fabrication

Microchannels were fabricated on silicon wafers using standard lithography and etching techniques. Silicon wafers (500  $\mu\text{m}$  thick, 100 mm diameter) were spin coated with a 3  $\mu\text{m}$  thick photoresist, lithographically patterned and etched using anisotropic dry reactive ion etching (DRIE) to create rectangular channels of the required depth. A 100 nm thick poly-tetra-fluoro-ethylene

(PTFE) layer was coated on some of the wafers to mimic the flow conditions in the fabrication process outlined in ref. 7.

### PDMS properties

The viscosity of liquid PDMS (Dow Corning Sylgard 184, 10:1 base to cross-linker ratio) reported in the literature is 3.9 Pa s.<sup>27</sup> However, because this is a reacting mixture, viscosity can change over time. The viscosity of PDMS with 10:1 ratio has been shown to increase by 8% from 4.15 Pa s to 4.48 Pa s over a 15 minute time span after 30 minutes of degassing.<sup>27</sup> In our study, all measurements were started within 10 minutes of mixing to minimize possible changes in viscosity.

A surface tension of 19.8  $\text{mN m}^{-1}$  at 20  $^{\circ}\text{C}$ <sup>28</sup> was used for PDMS. Goniometer measurements indicated an equilibrium contact angle of 30.4 $^{\circ}$  between PTFE-coated silicon and PDMS, while the equilibrium contact angle between uncoated silicon and PDMS was so small ( $<5^{\circ}$ ) that it could not be reliably measured. Therefore, a contact angle of 0 $^{\circ}$  was used in the model. Note that the equilibrium contact angle appears in the model as the argument in a cosine term, so this caused negligible error.

### Experimental procedure

A liquid PDMS droplet was injected within 10 minutes of mixing into a large reservoir (Fig. 1), which was connected to horizontal microchannels with nominal widths ranging from 5 to 50  $\mu\text{m}$ . After PDMS spread and impinged on the channels, the flows were recorded until the PDMS travelled about 3 mm in each channel. Video was recorded at 1 frame per second and converted to a sequence of images from which the location of the forward meniscus was tracked using digital image correlation in MATLAB<sup>TM</sup>. In microchannels with large widths and small depths, long fingers of PDMS often extended into the channel. In these cases, the cusp of the meniscus was tracked. Representative images of the meniscus cusp and liquid fingers are shown in Fig. 2.

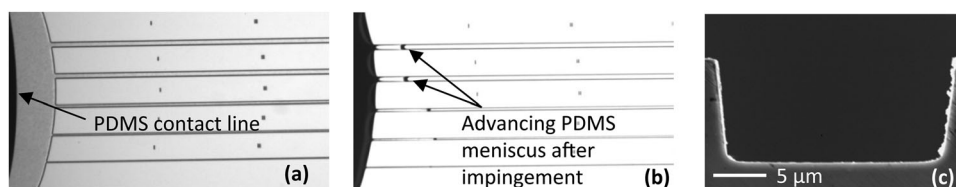


Fig. 1 (a) Channels with widths of 10, 20, 30, 40, and 50  $\mu\text{m}$ , from bottom to top. Liquid PDMS is visible in the reservoir on the left. (b) The channels after PDMS impingement. (c) Microchannel cross-section with 10  $\mu\text{m}$  depth and 20  $\mu\text{m}$  width.

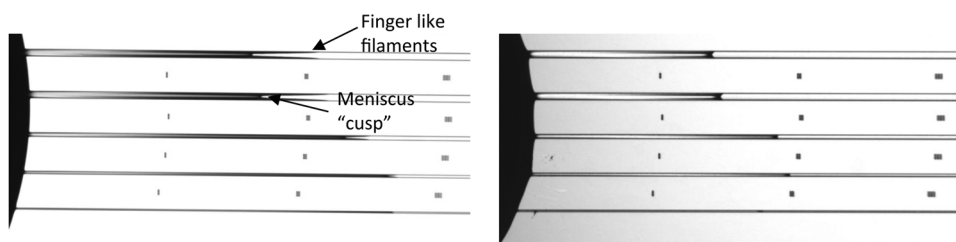


Fig. 2 Optical image of PDMS flow in PTFE coated microchannels with a depth of 10  $\mu\text{m}$  (left) and uncoated Si microchannels with a depth of 10  $\mu\text{m}$  (right). Variations in the forward meniscus length due to the surface coating and width to depth ratio are clearly seen.

The data was fitted to the equation  $x = a\sqrt{t}$  for capillary flow<sup>20,21</sup> with an offset for the initial time and meniscus location to derive the flow rate constant,  $a$ . For most channels (except those with very slow flow rates), only the data beyond the first 1.5 mm of the flow was considered for calculating  $a$ . This was done to avoid the initial transients and ensure that quasi-steady state conditions were satisfied, as assumed in the model. Three plots with experimental data and the generated fits are shown in ESI,† Fig. S1 for different combinations of surface coating, channel width, and channel depth. The  $R^2$  values for the fits were higher than 0.9985 on all 99 experiments having non-zero flow rates. The average of three experiments was used to calculate  $a$ , and error bands were defined by the maximum and minimum  $a$  value for a given experimental condition. The reactive ion etching caused a slight taper (due to process variability) in some of the microchannel sidewalls (Fig. 1c). To ensure that the taper did not cause a change in flow behaviour, we also fabricated channels using a different process (inductively coupled plasma DRIE) that produces nearly vertical channels. No meaningful differences were seen in the flow behaviour of PDMS in channels fabricated using the two methods.

### Model

The measured values of  $a$  were compared with values predicted by an analytical model<sup>25</sup> for capillary flow, based on the work of Lucas and Washburn.<sup>20,21</sup> In this model, Stokes' flow is assumed. Solving the governing equations while assuming a no

slip boundary condition on the bottom and sidewalls and a free slip boundary condition<sup>29</sup> on the top surface leads to a relation  $x^2 \approx kt = a^2t$ , where  $x$  is the distance travelled by the flow and  $t$  is the time.  $k$  is the "mobility parameter" given by

$$k = a^2 = \frac{2\gamma D}{\mu} \frac{2\cos\theta - (1 - \cos\theta)p}{p^2} g(p) \quad (1)$$

$k$  depends on the channel depth ( $D$ ), width ( $W$ ) and aspect ratio ( $p = W/D$ ), liquid surface tension ( $\gamma$ ), equilibrium contact angle ( $\theta$ ) and dynamic viscosity ( $\mu$ ).  $g(p)$  is a geometric parameter that is dependent only on the channel cross-section.

$$g(p) = \frac{128}{\pi^5} \sum_{n \geq 0, \text{ odd}} \frac{1}{n^5} \left[ \frac{n\pi}{4} p - \tanh\left(\frac{n\pi}{4} p\right) \right] \quad (2)$$

The model assumes that the channel is completely filled and the fluid has a flat top surface and forward (in the direction of the advancing flow,  $x$ ) meniscus. Thus, the velocity profile is taken to be dependent on the  $y$  and  $z$  direction only for a given pressure gradient. In addition, the model assumes that the contact angle is constant and equals the static equilibrium contact angle.

## 3. Results and discussion

The plots of  $a$ , which is a measure of the flow rate, versus  $p$  for uncoated and PTFE-coated Si microchannels are shown in Fig. 3 and 4, respectively. Flow rates on uncoated silicon wafers

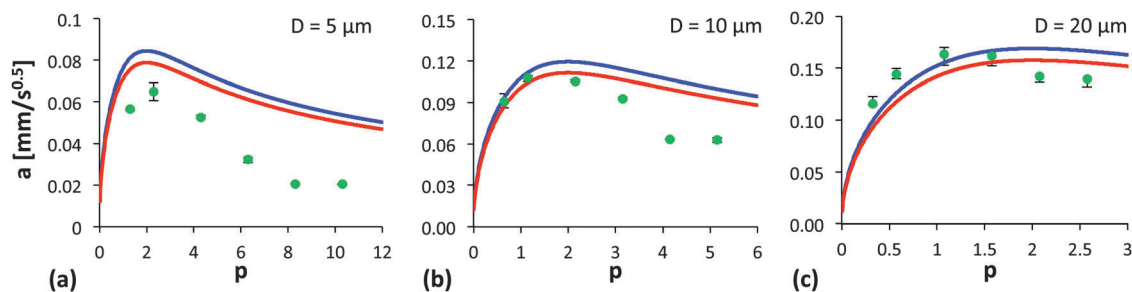


Fig. 3 Flow rate constant ( $a$ ) versus channel width to depth ratio ( $p$ ) for uncoated silicon microchannels with different channel depths ( $D$ ). The red and blue curves represent the model prediction with  $\mu = 4.48$  Pa s and  $\mu = 3.9$  Pa s, respectively, which represent the upper and lower bound of PDMS viscosity within the experimental timeframe. The green circles represent the mean value from 3 experimental measurements. The error bars represent the minimum and maximum values obtained.

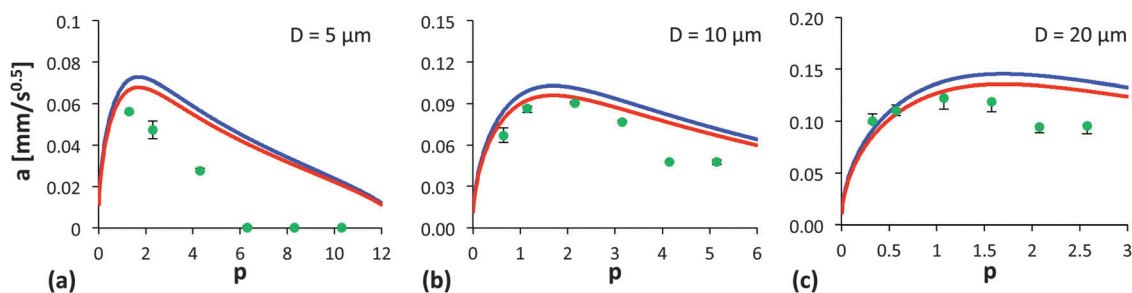


Fig. 4 Flow rate constant ( $a$ ) versus channel width to depth ratio ( $p$ ) for PTFE-coated silicon microchannels with different channel depths ( $D$ ). The red and blue curves represent the model prediction with  $\mu = 4.48$  Pa s and  $\mu = 3.9$  Pa s, respectively, which represent the upper and lower bound of PDMS viscosity within the experimental timeframe. The green circles represent the mean value from 3 experimental measurements. The error bars represent the minimum and maximum values obtained.

are higher by 20–50% compared to PTFE coated wafers when width and depth are held constant. This is expected because of the larger equilibrium contact angle (less tendency to wet) of PDMS on PTFE-coated wafers. The plots also show that  $a$  varies with  $p$  for a given surface coating.

When  $p < 1$ , the fluid flow rate reduces due to higher viscous forces caused by the steeper velocity gradients in narrow channels. When  $p$  becomes large, the flow rate again decreases substantially because the ratio of the capillary driving force (proportional to the surface area) to the volume of fluid drawn into the channel (proportional to the cross-sectional area) becomes smaller. This happens because the relative contribution of the sidewalls to the surface area becomes smaller at larger  $p$ . Thus, there exists an intermediate  $p$  where the experimental and predicted values of  $a$  attains a maximum. For most channels this “ideal” width to depth ratio appears to be around 2. More importantly, while the model predictions and experimental measurements compare reasonably well for small values of  $p$ , they increasingly diverge as  $p$  increases. In particular, as  $p$  increases for a given depth, the experimental flow rates tend to progressively lag relative to the model. Note that the Reynolds number for even the fastest flows in our experiments is less than  $10^{-6}$ . Therefore, the conditions for Stokes’ flow are satisfied and it is appropriate to compare the experimental results with those from the model.

Two factors could explain the lag in experimental flow rates relative to model predictions as  $p$  increases. The first factor is the upper meniscus morphology. In the channels that exhibit non-zero flow rates, the meniscus has a concave profile (Fig. 5) and hence the effective depth of the fluid is less than the channel depth. Therefore, the velocity gradient is steeper and the drag due to shear stress is significantly higher. This leads to a reduced flow rate as compared to the model prediction, which assumes a fully filled channel. For a given channel depth, the effect of the concave upper meniscus becomes more

pronounced at larger widths (Fig. 5). Similarly, for a given width the effect is most acute for the shallower channels.

To better illustrate the effect of the upper meniscus morphology, we used eqn (1) to non-dimensionalize the flow rate constant  $a$  (dividing by  $\sqrt{\frac{\gamma D}{\mu}}$ ) and plotted the results (Fig. 6) as a function of  $p$  for both uncoated and PTFE coated channels. If the experiments followed the model predictions, this non-dimensional flow rate constant would depend only on  $p$  and  $\theta$  and not on the channel dimensions. But as evident from the results in Fig. 6, this is clearly not the case. The deeper channels (10 and 20  $\mu\text{m}$ ) consistently show higher values compared to the shallow channel (5  $\mu\text{m}$ ), where the effect of the top meniscus is most pronounced.

The second factor responsible for the fluid flow lag is the forward meniscus morphology, which is also not taken into account in the analytical model. As described in ref. 30, these meniscus morphologies depend only on the equilibrium contact angle ( $\theta$ ) and  $p$ . In our experiments, a curved forward meniscus develops in which the fluid height gradually decreases and finger-like filaments protrude at the bottom corners of the channels. Due to the small distance between the channel wall (no slip) and the inner finger edge, viscous force in the fingers is large, which leads to a reduction in flow rates. The finger-like protrusions are typically longer in channels with large  $p$  (Fig. 2), which can explain why the experimental flow rates lag more as  $p$  becomes larger.

To complement these experimental observations, we also numerically simulated the meniscus profiles using Surface Evolver,<sup>31</sup> which employs an iterative technique to minimize the surface energy and obtain the equilibrium meniscus shape. Surface Evolver codes were written to generate spontaneous capillary flow conditions for PDMS flow in microchannels with varying aspect ratio. The simulations (Fig. S2, ESI†) showed that the finger-like filaments progressively become longer at larger aspect ratios, confirming the experimental observations.

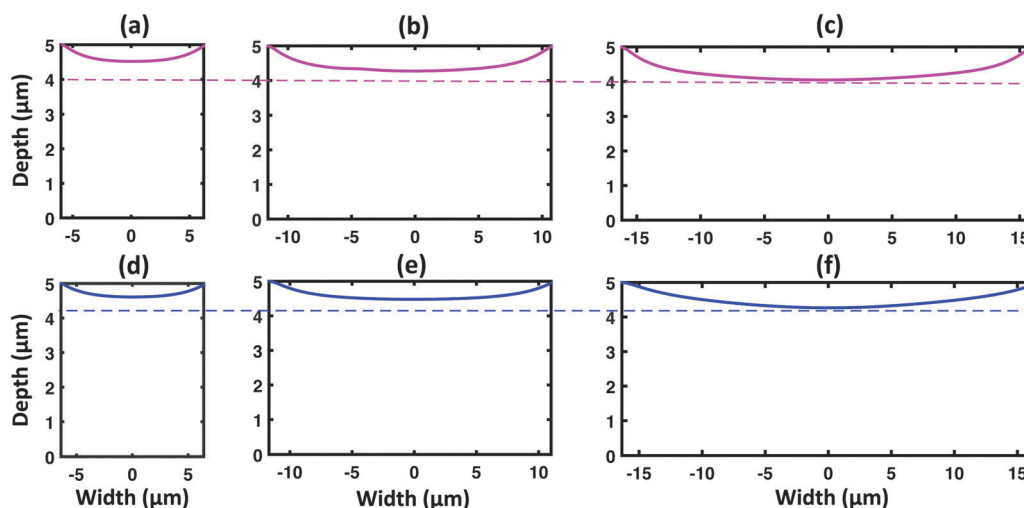


Fig. 5 Upper meniscus profile of PDMS in 5  $\mu\text{m}$  deep microchannels with different widths measured using an atomic force microscope. (a–c) Uncoated Si microchannels. (d and e) PTFE coated microchannels. The dashed line coincides with the lowest point of the meniscus in the widest channel and illustrates the reduced effective channel depth as the width increases.

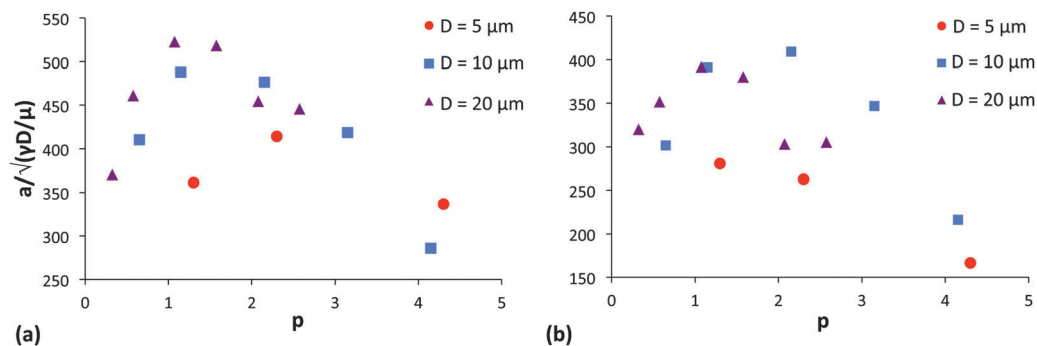


Fig. 6 Non-dimensional flow rate constant ( $a/\sqrt{\gamma D/\mu}$ ) versus  $p$  for (a) uncoated Si microchannels and (b) PTFE-coated microchannels. The non-dimensional flow rate constant is smallest for the shallowest channel ( $D = 5 \mu\text{m}$ ), reflecting the more pronounced effect of the concave upper meniscus.

Apart from the effect of the upper and forward meniscus, the change in contact angle with flow velocity could also be responsible for the discrepancy between the model and experimental results. In the model, a constant static contact angle is assumed for the flow. If the dynamic contact angle was taken into account,<sup>32</sup> it would have the effect of lowering the flow rate constant ( $a$ ) predicted by the model and potentially lead to a closer agreement with our experimental data. But as shown in ref. 25, an excellent agreement between the model and experiments is obtained when meniscus effects are negligible, even if the dynamic contact angle is not considered. This suggests that changes in the dynamic contact angle are not the primary reason for the discrepancy between model predictions and experiments in our study. Similarly, non-Newtonian behavior (variation of viscosity with shear rate) of PDMS also cannot account for the differences between the model and experiments. The viscosity of PDMS has been shown to increase from  $\sim 4.05 \text{ Pa s}$  to  $\sim 4.15 \text{ Pa s}$  as the shear rate is varied from  $0.01/\text{s}$  to  $30/\text{s}$ .<sup>27</sup> In our experiments, the estimated maximum shear rate (assuming 1D parabolic flow profile) is below  $2/\text{s}$  under quasi-steady state conditions, even for the fastest flows in the narrowest channels. This shear rate translates to a viscosity ( $\mu$ ) change of less than 0.5%, and since the flow rate constant ( $a$ ) varies as the inverse square root of  $\mu$  (eqn (1)), the results would essentially remain unchanged.

Another notable aspect of PDMS flow behaviour in our experiments is the zero flow rate in  $5 \mu\text{m}$  deep PTFE-coated channels ( $\theta = 30.4^\circ$ ) with widths  $> 30 \mu\text{m}$  (Fig. 5(a)). Based on the analysis in ref. 30, only protruding filaments are expected to form in these channels for  $\theta = 30.4^\circ$ , which is confirmed by the experiments. We also note that the lack of PDMS incursion in this regime is consistent with multiple experimental studies<sup>33–35</sup> in which fluids are made to extend or retract in microfluidic channels *via* manipulation of their equilibrium contact angle.

## 4. Conclusions

In summary, experimental measurements of PDMS flow in open rectangular silicon microchannels are compared to an analytical model.<sup>25</sup> The experimental flow rates show varying degrees of agreement with model predictions depending on

channel aspect ratio. The differences can be mostly accounted for by changes in forward and upper meniscus morphology, and the consequent changes in viscous dissipation, as channel aspect ratio is varied. The results strongly suggest that forward and upper meniscus morphology must be taken into account to accurately predict capillary driven flow, especially in shallow channels with large aspect ratios. Nevertheless, the square root dependence of flow distance on time is preserved even in large aspect ratio channels. This suggests that the underlying physics of the flow is not fundamentally altered by the change in boundary conditions.

In addition, a few rules of thumb for fabricating PDMS devices *via* capillary micromolding can be inferred from the study. First, it is preferable to have channels with aspect ratios near two to ensure full impingement of PDMS into the device mold. Second, aspect ratios larger than three should be used sparingly, even though a large aspect ratio may be desirable to reduce the out-of-plane stiffness of force sensors.<sup>7</sup> Finally, the channel geometries that would lead to zero PDMS impingement<sup>30</sup> should be avoided.

## Acknowledgements

This research was based upon work supported by the National Science Foundation grants ECCS 1102201, CMMI 1400505 and DMR 1454109 and a seed grant from Arizona State University. We gratefully acknowledge the use of facilities with the LeRoy Eyring Center for Solid State Science and the Center for Solid State Electronics Research at Arizona State University. We are also thankful to Kenneth A. Brakke (Susquehanna University) for helping us with the numerical simulations in Surface Evolver.

## References

- 1 S. Quake and A. Sherer, *Science*, 2000, **290**, 1536.
- 2 X. Tang, P. Bajaj, R. Bashir and T. Saif, *Soft Matter*, 2011, **7**, 6151.
- 3 I. Levental, P. Georges and P. Janmey, *Soft Matter*, 2007, **3**, 299.
- 4 R. Tran, P. Thevenot, D. Gyawali, J. Chiao, L. Tang and J. Yang, *Soft Matter*, 2010, **6**, 2449.

- 5 M. Liu, J. Sun, Y. Sun, C. Bock and Q. Chen, *J. Micromech. Microeng.*, 2009, **19**, 1.
- 6 Dow Corning Sylgard 184 Product Sheet.
- 7 J. Rajagopalan and M. T. A. Saif, *J. Microelectromech. Syst.*, 2013, **22**, 992.
- 8 Y. Zhao and X. Zhang, *Appl. Phys. Lett.*, 2005, **87**, 144101.
- 9 J. Tan, J. Tien, D. Pirone, D. Gray, K. Bhadriraju and C. Chen, *Proc. Natl. Acad. Sci. U. S. A.*, 2003, **100**, 1484.
- 10 A. K. Harris, D. Stopak and P. Wild, *Nature*, 1981, **290**, 249.
- 11 J. Park, J. Ryu, S. K. Choi, E. Seo, J. M. Cha, S. Ryu, J. Kim, B. Kim and S. H. Lee, *Anal. Chem.*, 2005, **77**, 6571.
- 12 Y. Zhao, C. C. Lim, D. B. Sawyer, R. Liao and X. Zhang, *Cell Motil. Cytoskeleton*, 2007, **64**, 718.
- 13 D. Kim, P. K. Wong, J. Park, A. Levchenko and Y. Sun, *Annu. Rev. Biomed. Eng.*, 2009, **11**, 203.
- 14 J. Rajagopalan and M. T. A. Saif, *J. Micromech. Microeng.*, 2011, **21**, 054002.
- 15 G. M. Whitesides, E. Ostuni, S. Takayama, X. Jiang and D. E. Ingber, *Annu. Rev. Biomed. Eng.*, 2001, **3**, 335.
- 16 R. Bashir, *Adv. Drug Delivery Rev.*, 2004, **56**, 1565.
- 17 B. J. Williams, S. V. Anand, J. Rajagopalan and M. T. A. Saif, *Nat. Commun.*, 2014, **5**, 3081.
- 18 K. Enoch, Y. Xia and G. M. Whitesides, *Nature*, 1995, **376**, 581.
- 19 K. Enoch, Y. Xia and G. M. Whitesides, *J. Am. Chem. Soc.*, 1996, **118**, 5722.
- 20 R. Lucas, *Kolloid-Z.*, 1918, **23**, 15.
- 21 E. W. Washburn, *Phys. Rev.*, 1921, **17**, 273.
- 22 W. Ryu, Z. Huang, J. S. Park, J. Moseley, A. R. Grossman, R. J. Fasching and F. B. Prinz, *Lab Chip*, 2008, **8**, 1460.
- 23 F. F. Ouali, G. McHale, H. Javed, C. Trabi, N. J. Shirtcliffe and M. I. Newton, *Microfluid. Nanofluid.*, 2013, **15**, 309.
- 24 S. Girardo, S. Palpacelli, A. De Maio, R. Cingolani, S. Succi and D. Pisignano, *Langmuir*, 2012, **28**, 2596.
- 25 D. Yang, M. Krasowska, C. Priest, M. N. Popescu and J. Ralston, *J. Phys. Chem. C*, 2011, **115**, 18761.
- 26 R. H. Nilson, S. K. Griffiths, S. W. Tchikanda and M. J. Martinez, *Int. J. Heat Mass Transfer*, 2006, **49**, 1603.
- 27 F. Schneider, J. Draheim, R. Kamberger and U. Wallrabe, *Sens. Actuators, A*, 2009, **151**, 95.
- 28 A. P. Robinson, I. Mineev, I. M. Graz and S. P. Lacour, *Langmuir*, 2011, **27**, 4279.
- 29 L. Parkinson, R. Sedev, D. Fornasiero and J. Ralston, *J. Colloid Interface Sci.*, 2008, **322**, 168.
- 30 R. Seemann, M. Brinkmann, E. J. Kramer, F. F. Lange and R. Lipowsky, *Proc. Natl. Acad. Sci. U. S. A.*, 2005, **102**, 1848.
- 31 K. A. Brakke, The surface evolver, *Exp. Math.*, 1992, **1**, 141.
- 32 M. N. Popescu, J. Ralston and R. Sedev, *Langmuir*, 2008, **24**, 12710.
- 33 J. Baret, M. Decre, S. Herminghaus and R. Seemann, *Langmuir*, 2005, **21**, 12218.
- 34 J. Baret, M. J. Decre, S. Herminghaus and R. Seemann, *Langmuir*, 2007, **23**, 5200.
- 35 K. Khare, S. Harminghaus, J. Baret, B. Law, M. Brinkmann and R. Seemann, *Langmuir*, 2007, **23**, 12997.